Ammoniated Aqueous Precursor Ink Processed Copper Iodide as Hole Transport Layer for Inverted Planar Perovskite Solar Cells

Dhruba B. Khadka*[12], Yasuhiro Shirai[3**], Masatoshi Yanagida[3], Kenjiro Miyano[3]

[1] Interfacial Energy Conversion Group, Center for GREEN Research on Energy and Environmental Materials, National Institute for Materials Science (NIMS), 1-1 Namiki, Tsukuba, Ibaraki 305-0044, Japan.

[2]International Center for Young Scientists (ICYS), National Institute for Materials Science (NIMS), 1-1 Namiki, Tsukuba, Ibaraki 305-0044, Japan.

[3]Global Research Center for Environment and Energy based on Nanomaterials Science (GREEN), National Institute for Materials Science (NIMS), 1-1 Namiki, Tsukuba, Ibaraki 305-0044, Japan.

Corresponding Author

*E-mail: KHADKA.B.Dhruba@nims.go.jp

**E-mail: SHIRAI.Yasuhiro@nims.go.jp

Abstract

The inorganic carrier transport layers are robust and stable to the environment compared to the organic hole transport layer (HTL). Here, we report on the fabrication of the halide perovskite solar cells (HaPSCs) employing CuI deposited with ammoniated aqueous solution ink as HTL and explored the material properties and device characteristics. The film morphology of CuI is found to have an influence on the HaP film growth and hence effects on the device parameters. The HaPSC with CuI has demonstrated the power conversion efficiency of ~14.21% with high reproducibility. The capacitance spectra analysis shows that the deep trap states are induced in the perovskite absorber layer. The results obtained from the temperature-dependent open circuit voltage implicates that the recombination activities in the perovskite bulk are dominant. Furthermore, the HaPSC with CuI has revealed better air stability compared to the device with PEDOT:PSS. This work suggests that the CuI processed with aqueous precursor is a promising alternative HTL to PEDOT:PSS for efficient and stable perovskite solar cells as well as in a tandem device.

Key words: Halide perovskite, copper iodide, interface recombination, capacitance spectra

1. Introduction

Halide perovskite (HaP) materials have demonstrated an unprecedented progress with device power conversion efficiency (PCE) ~25% owing to excellent optical and electronic properties.[1–3] Although the material growth and device fabrication approaches have rapidly progressed, there is still much room to improve the device performance to achieve device parameters close to theoretical estimation.[4] The carrier transport layers (CTLs) are crucial for the high quality perovskite thin film besides getting optimal band alignments,[5] to get high PCE and longer the device stability.[6,7] The film quality and stability of perovskite devices are affected by the nature of CTL on which perovskite film is grown.[8,9] In the inverted structure, the organic HTL; PEDOT:PSS and PTAA are popularly used in HaPSCs. But the high cost of PTAA and device deterioration due to the acidic and hygroscopic nature of PEDOT:PSS may impose a barrier for cost-effective large production. Considering these issues, the inorganic HTLs are potential alternatives due to the low cost, high conductivity, robustness, and air stability. Multiple groups have reported promising device performance with significantly improved device stability using the inorganic HTLs.[9–11] The transition metal oxides HTLs; NiO_x,[10] doped-NiO_x,[12–14] CuO_x,[15,16] and VO_x[17] have demonstrated an efficient and stable device in the inverted HaPSCs.

Furthermore, the inorganic copper-based p-type HTLs such as copper iodide (CuI) and copper thiocyanate (CuSCN), have also used as promising alternatives due to their excellent optoelectrical properties as well as low production cost and solution processability. They

have widely used as HTLs in the organic[18,19] and dye-sensitized solar cells.[20] There are also few reports using CuI[21–23] or CuSCN[24,25] as HTL in the inverted HaPSC with competitive device efficiency and stability. It is to be noted that the CuI precursor solution has been prepared in toxic organic solvents;[26] such as acetonitrile, [27,28] and diethyl sulfide[23,29] which are unfavorable for the deposition under ambient conditions. Therefore, the HTL precursor ink with a non-toxic solvent is also important to minimize the health hazard during the processing of HTL film in ambient conditions. In addition, the exploration of the perovskite device with the inorganic HTLs is crucial to understand the effect of inorganic HTL on the perovskite film and device parameters.

In this work, we have fabricated the HaP device of inverted configuration using CuI as HTL. We have used ammoniated aqueous precursor ink of CuI in place of the toxic solvent.[26] The ammoniated aqueous solution ink processed CuI film and perovskite layer were characterized to investigate the material growth. The device with CuI was found to be affected by CuI morphology tailored with precursor concentration. The analysis of current-voltage characteristics and capacitance spectroscopy (*C-f*) suggests that the CuI device suffers from the recombination activities in the perovskite bulk. We found rather deep trap states induced in the perovskite layer grown on the CuI during film crystallization. The HaPSC with CuI demonstrated superior stability compared to the aqueous PEDOT:PSS based device.

2. Experimental

2.1. Device fabrication

We have purchased all chemicals from commercial suppliers as mentioned and unless otherwise specified, they were used as received. We prepared the copper iodide (CuI) (Sigma Aldrich, 99% purity) precursors of 0.025, 0.05, and 0.1 M concentrations by dissolving in de-ionized water and ammonium solution in 9:1 ratio (Fig. S1). Note that CuI powder is readily soluble in de-ionized water (DIW) as depicted in Fig. S1. The thin CuI films (30-50 nm) were deposited onto the ITO substrate by spin coating (3000 rpm for 30 sec and 140 ℃ for 45 min in air ambient) as described in our report.[30] $CH_3NH_3PbI_{3-x}Cl_x$ perovskite films were prepared by spin coating the PbI_2 precursor solution with subsequently dripping a mixed precursor solution of MAI + MACl. Then, the perovskite films were crystallized by annealing with MACl powder covered with a petri dish at 100 ℃.[31] After that, Phenyl C_{61} butyric acid methyl ester ($PC_{61}BM$) [Sigma Aldrich, 99% purity] (20 mg/ml in chlorobenzene) was used for the electron transport layer (ETL). Aluminum doped zinc oxide (AZO) nanoparticle ink (Nanograde N-21X) (100 μl, 2500 rpm-20 sec dynamic coating, annealing at 100 ℃ for 5 min) was used to prepare an AZO layer. Finally, Ag (100 nm) was thermally evaporated and get a device of ~0.26 cm^2 area. Devices were sealed using UV-curable resins before the subsequent measurements in ambient conditions.

2.2. Materials and device characterizations

The XRD patterns were collected using Rigaku Smart Lab, CuK_α radiation, λ=1.5405Å. The SEM images were obtained using a high-resolution scanning electron microscope at 5kV accelerating voltage (Hitachi, S-4800). The absorption spectra and photoluminescence (PL) spectra of various films were measured using UV-Vis-NIR spectrometer (7200, V-Jasco) and Spectrofluorometer (FP8500, Jasco). The current density–voltage (*J*–*V*) curves were

measured at the scan rate of 0.05V/s under 1 sun with an AM1.5G spectral filter (100 mW/cm^2) coupled with an MPPT system (Systemhouse Sunrise Corp.). For the stability test, the encapsulated devices were measured at MPPT (Maximum Power Point Tracking) conditions at ~30 ℃ under relative humidity (RH) ~ 50 %. The external quantum efficiency (EQE) spectra were obtained using a spectrometer (SM-250IQE, Bunkokeiki, Japan). Capacitance–frequency response (*C–f*) was obtained using an LCR meter (IM3536, Hioki), which probes from 20 Hz to 2 MHz at the AC voltage amplitude of 30 mV under dark conditions in the temperature range of 253 K−343 K. After confirming the geometric capacitance regime in *C–f* spectra, capacitance-voltage (*C–V*) measurements were carried out at 10 kHz under dark condition (the geometric capacitance regime in C–f spectra). For temperature-dependent *C−f* scans, a temperature-controlled chamber (SU-221) was used having a control system with an error of ±0.1 K (℃).

3. Results and discussion

We noticed that the CuI precursor ink prepared in de-ionized water (DIW) readily dissolves as depicted in supporting information (Fig. S1). In previous reports, CuI precursor has been prepared in toxic organic solvents such as acetonitrile, [27,28] and diethyl sulfide.[23] On surging a non-toxic solvent, it is found that the CuI powder is well dissolved in ammoniated de-ionized water (DIW). As ammonia is added, CuI dissolved as Cu^+ ion forms a complex with ammonia [($CuI + 2NH_3$ (aq) ↔ $Cu(NH3)_2^+ + I^-$ (aq)] giving a deep blue precursor ink (Fig. S1). This approach is much safe to process it under ambient conditions.

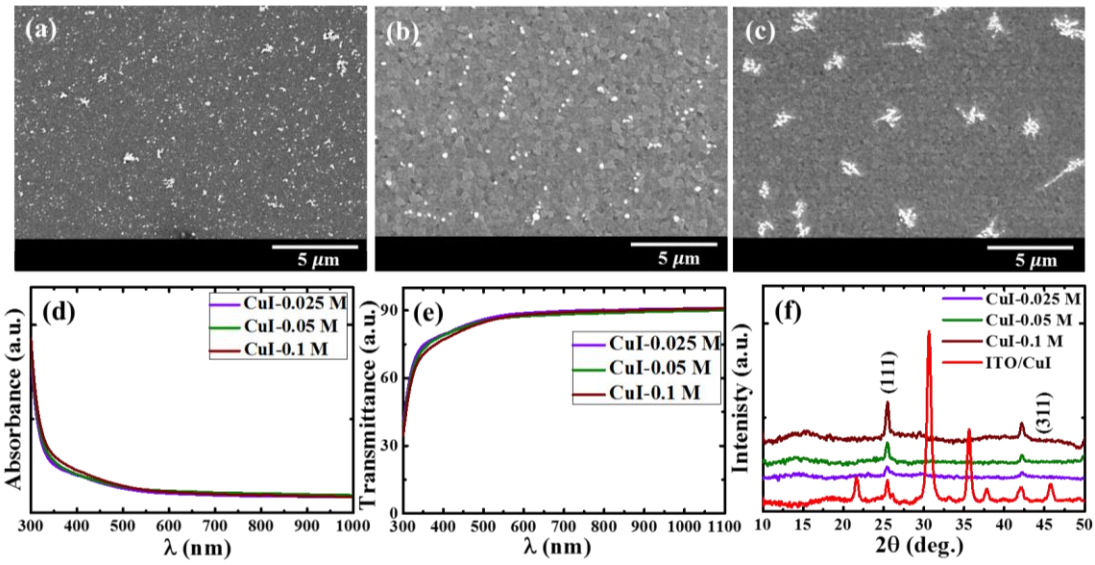

Figure 1. The surface texture of CuI films deposited with CuI precursors of different concentrations (a) 0.025 M, (b) 0.05 M, and (c) 0.1 M. The absorption spectra (d), transmission spectra (e), and XRD patterns (f) of respective films.

Figures 1 (a-c) show the morphology of CuI films deposited with different concentration of precursor solution. The CuI film of 0.05 M exhibits smooth morphology with larger grain size whereas the CuI film of 0.1 M has a comparatively rough surface that appears as white spots. The thickness of CuI film is in the range of 25-50 nm (25 $\pm$ 5 nm, 35 $\pm$ 5 nm, and 50$\pm$ 5 nm for the CuI film deposited with the precursor of 0.025, 0.05, and 0.1 M, respectively) showing a slight dependence on precursor concentration. The absorption and transmission spectra (Fig. 1d, e) exhibit almost similar features with slightly varying responses for the CuI film deposited with higher precursor concentration. Note that transmittance spectra for the CuI films are higher in the regime of beyond $\geq$450 nm spectrum compared to aqueous processed PEDOT:PSS (Fig. S2) which is beneficial to get more light illumination in the HaP absorption range. The ultraviolet photoelectron yield spectra (Fig. S3) estimate the HOMO

level at 5.30± 0.02 eV. This is in the range of other reports.[28] The XRD patterns of CuI films (Fig. 1d) exhibit the characteristic peaks with orientations (111) and (311).[27,32] The difference in intensity is attributed to the film quality as well as the thickness of CuI films.

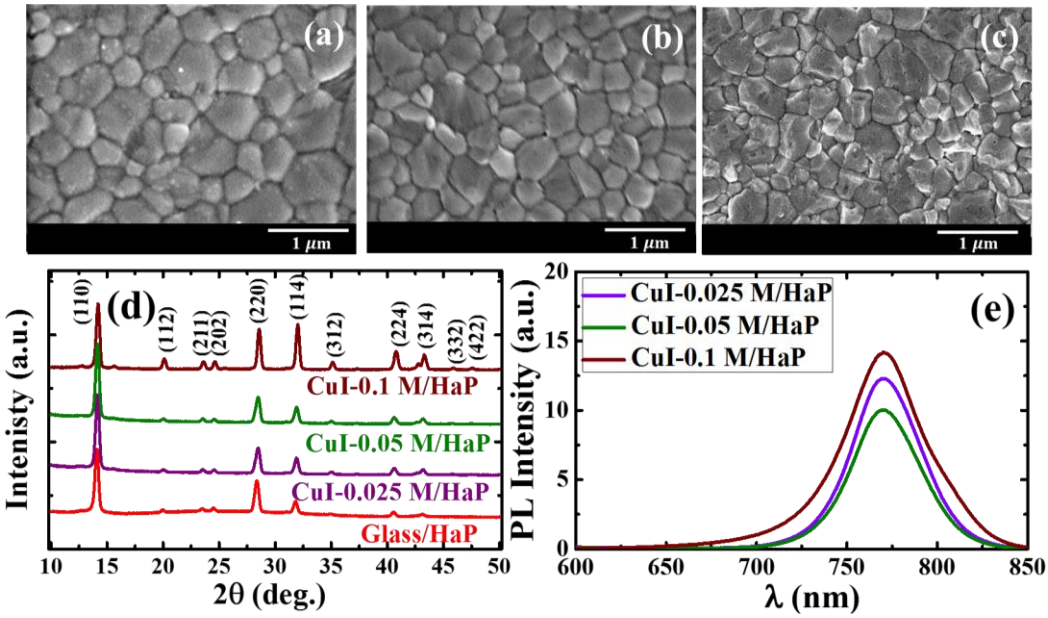

Figure 2. The morphology of perovskite film grown on CuI films deposited with CuI precursors of (a) 0.025 M, (b) 0.05 M, and (c) 0.1 M. The XRD patterns (d) and PL spectra (e) of the respective films.

Figures 2 (a-c) show the morphology of perovskite films grown on those CuI films with different concentration of precursor solution. The perovskite films grown on respective CuI HTLs are found to be affected by the surface texture of the CuI film. The perovskite film on CuI with 0.05M (Fig. 2b) consists larger and uniform grain size whereas that on 0.1 M CuI film possesses more grain boundaries with small crystallites. The XRD patterns of perovskite films grown on the CuI layer show high crystallinity with characteristic orientations.[33] Note that the XRD patterns of the perovskite grown on the CuI film of 0.1 M exhibited a

relatively higher intensity of (220) and (114) crystal orientations. The PL spectra (Fig. 2e) reveal slightly higher PL quenching for 0.05 M-CuI/HaP film with comparatively narrower FWHM suggesting more efficient carrier transport and better film quality. The normalized absorption and PL spectra (Fig. S4a) demonstrated well matched opto-physical response at the band edge. The difference in PL response from the back and front side illumination on the glass/CuI/HaP/PMMA film must be related to the different interface quality formed at the HaP interface with the adjacent layer.

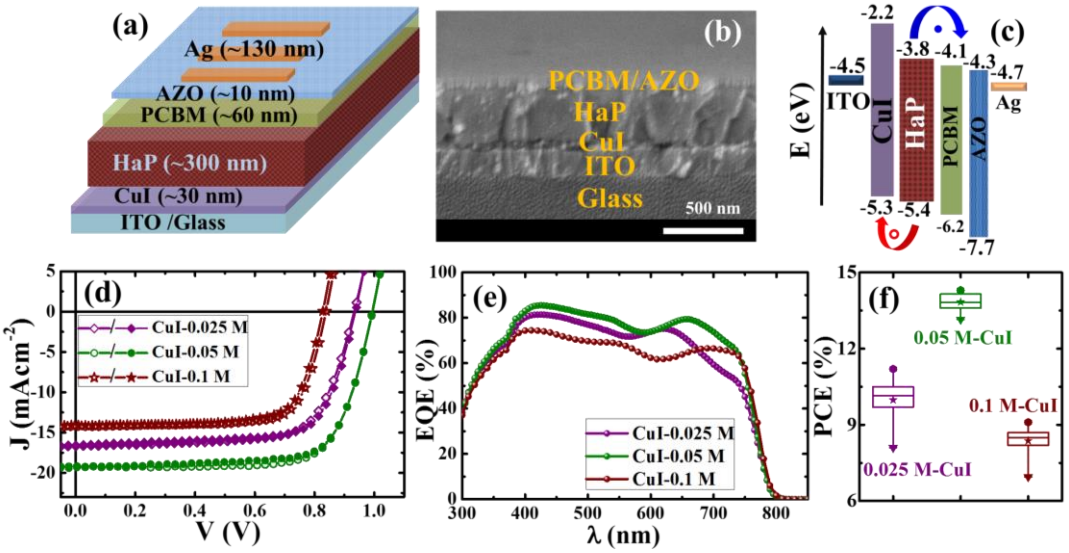

Figure 3. Schematic illustration of the device structure (a), cross-sectional image, and (c) energy band diagram of the device. J-V curves (d), EQE responses (e), and device statistics (f) of the HaPSCs with respective CuI layers prepared with aqueous solution of different concentrations (0.025, 0.05, and 0.1 M). Note that the filled and unfilled symbol in J-V curves represents forward and reverse scan direction.

Table1. Device parameters/properties of the HaPSCs with aqueous ammonia precursor of the CuI having different concentrations. The best device parameters are displayed outside

the parentheses. The tabulated value in in parentheses are the average values and standard deviation (20 devices from 4 batches) of respective devices.

Device parameters/ CuI film	0.025 M- CuI	0.05 M- CuI	0.1 M- CuI
	25 ± 5 nm	35 ± 5 nm	50 ± 5 nm
J_{sc}(mAcm^{-2})	16.55 (14.75±2.20)	19.39 (18.86±1.30)	14.04 (13.65±1.85)
V_{oc} (V)	0.93 (0.90±0.05)	0.99 (0.96±0.04)	0.84 (0.80±0.06)
FF	0.72 (0.67±0.05)	0.74 (0.71±0.03)	0.73 (0.70±0.04)
R_s (Ω·cm^2)	6.03 (7.62 ±2.05)	5.06 (6.02 ±1.53)	5.96 (6.87 ±2.42)
R_{sh} (kΩ·cm^2)	0.77 (0.45 ±0.16)	25.8 (21.35 ±2.65)	2.26 (1.86 ±1.05)
η (%)	11.10 (10.20±1.2)	14.21 (13.65±1.1)	8.83 (6.78±1.5)

Figure 3a depicts the schematic of HaPSCs structure with an energy band diagram (Fig. 3c) having the CuI as an HTL and PCBM as an ETL coupled with a thin Al:ZnO (AZO) as an electron selective layer (ESL) beneath the Ag electrode. Figure 3b displays the cross-sectional image of HaPSC with CuI. The current density-voltage (*J-V*) characteristics (Fig. 3d) and corresponding device parameters (Table 1) show the device results. The device with CuI deposited with the precursor of 0.05 M concentration demonstrated a higher device efficiency of ~14.21 % (the steady-state of J_{SC} and PCE; Fig. S5) with higher J_{SC} ~19.39 mAcm^{-2} and V_{OC} ~0.99 V. This result is competitive to the reported device performance using CuI.[19,34] The device parameters are also more scattered compared to CuI deposited with 0.05M-CuI precursor (Fig. 3f). The devices with CuI film (0.025 or 0.1 M) demonstrate comparatively poor device parameters (V_{OC} and J_{SC}), this is concurrent with higher R_s and lower R_{Sh}. This is partially attributed to the morphology of the CuI and HaP film (Fig. 1, 2). We can notice the surface texture of CuI film with a small island. This effects on the morphology of perovskite film which causes the leakage current and small *Rsh*.[8,27]. It has been documented that the thickness and HOMO level of HTLs impact on the device

parameters.[29,35,36] Thus, it is speculated that the variation on the thickness and HaP film quality induced by CuI film quality (morphology and optophysical properties) affect the V_{OC} and J_{SC} values of the respective devices.

The external quantum efficiency (EQE) spectra of respective devices are displayed in Fig. 3e. The integrated J_{SC} values obtained from respective EQE spectra are 16.48, 19.32, and 13.96 mAcm^{-2} for the devices with 0.025, 0.05, and 0.1 M- CuI HTL, respectively. These are in the agreements with the values of J_{SC} from *J-V* curves. We observe a slight change in the EQE response in the short wavelength regime (~300- 400 nm). This could be related to the thickness and quality difference of the CuI film. The spectral responses above 400 nm regime demonstrates a significant difference. This is the consequence of an improvement in the film quality and interface at HTL.[23,30]

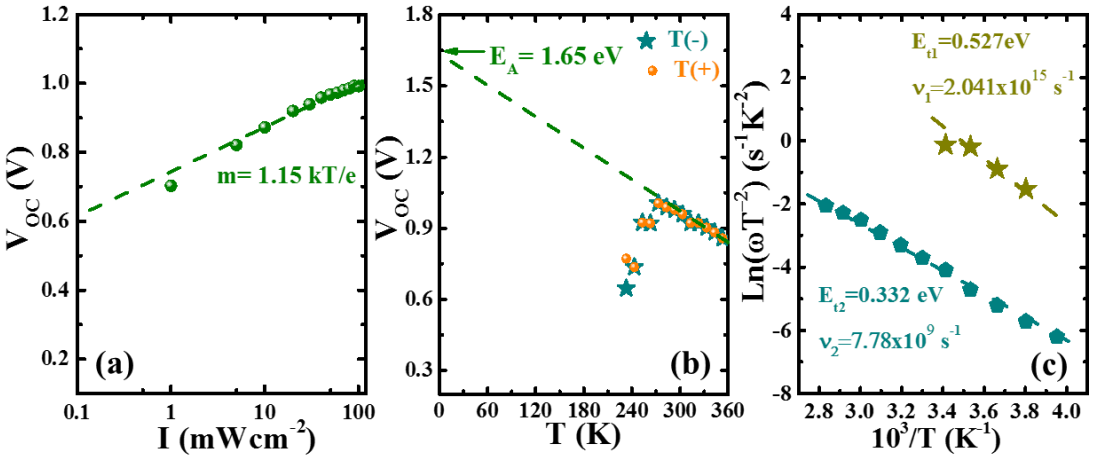

Figure 4. Plots of V_{OC} with varying light intensity (I) (V_{OC}-*I*) (a) and temperature (V_{OC}-*T*) of the HaPSC with CuI (0.05 M) (the best device). The Arrhenius plot (c) extracted from temperature-dependent capacitance-frequency (*C-f-T*) spectra. Here, the dashed lines

represent a linear fit for the respective plots. The T(+) and T(-) in plot (b) stand for measurement taken with increasing and decreasing temperature, respectively.

To get insight into the HaPSC with CuI as HTL, the devices with 0.05 M-CuI having the best device performance are used for analysis. We measure the light intensity (I) dependent *J-V* characteristics (*J-V-I*) (Fig. S6a). The analysis of the V_{OC}-*I* plot gives a clue about the recombination mechanism of the photogenerated charge carrier in the device.[37] A semilogarithmic plot V_{OC} as a function of light intensity (*I*) (Fig. 4a) showed a slope of 1.15 kT/e. This suggests the occurrence of trap-assisted recombination under device operation.[37] In addition, the energy shift ($\Delta E = Eg - E_1$; E_1 is an intercept of V_{OC}-*I* plot)[31],[37] is calculated to be 0.675 eV. This energy shift is indicative of energetic disorder in the device at the perovskite/CuI interface. The value of energy shift is lower than the PEDOT:PSS in our previous report[38] suggesting that CuI has a better interface junction.

To understand the recombination activities further, the temperature dependent *J-V* characteristics (Fig. S6b) were taken in the temperature range of 233 to 353 K. Despite hysteresis free *J-V* curve at room temperature (Fig. 3d), it is predominantly observed at low temperature *J-V* curve (Fig. S6b) which is analogous to the earlier report.[39] Interestingly, the HaPSC with CuI exhibited a varying V_{OC} or J_{SC} with the scan direction at low temperature *J-V* characteristics. It is attributed to the pining of interfacial or bulk traps or contact limited problem at low temperature device operation.[40] In addition, from the V_{OC}-*T* plot, we can extract the activation energy of the dominant recombination process, E_A.[38] It is to be noted that the value of E_A with respect to Eg implicates the strength of the defect-mediated recombination at the interface or in the bulk of perovskite layer.[41] The value of E_A can be

estimated by the linear extrapolation of V_{OC}-T plots (Fig. 4b) to 0 K. This result (E_A~1.65 eV~ E_g) indicates that recombination activity in the perovskite layer bulk is rather dominant. It also agrees with the result of the intensity dependent V_{OC} analysis.

Furthermore, to explore the defect activities in the perovskite bulk, the temperature-dependent capacitance spectra were analyzed to estimate the trap centers within the bandgap.[9,42] The Arrhenius plot and defect density are extracted from the temperature dependent capacitance frequency (*C-f-T*) spectra as discussed in the earlier reports,[31,42,43] The *C-f-T* spectra for HaPSC with the CuI as HTL are displayed in Fig. S6c,d. The trap states in the CuI device estimated to be 0.332 and 0.527 eV from the analysis of the Arrhenius plot (Fig. 4d) extracted from the *C-f-T* spectra. These traps are rather deeper. This is attributed to the Cu antisites induced in the perovskite layer due to diffusion of the Cu ions during device processing. The trap densities in the perovskite bulk are calculated to be in the range of 10^{16}-10^{17} cm^{-3}. These trap centers cause the recombination activities in the HaP bulk. This is detrimental to the improvement in device parameters.

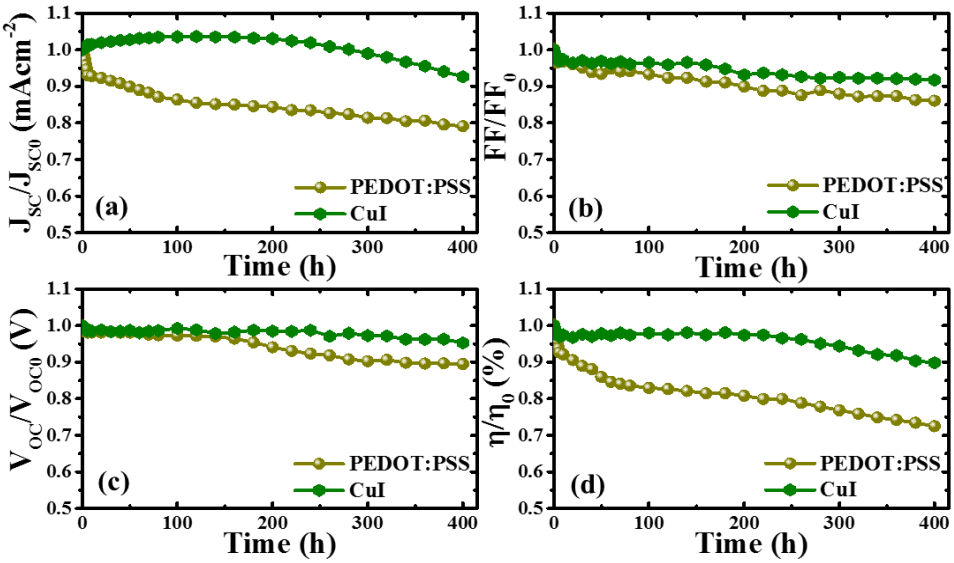

Figure 5. Stability data for device parameters (normalized) of encapsulated devices with CuI or PEDOT:PSS; aqueous precursor under continuous illumination. The device was kept under MPPT condition between the periodical J-V measurements.

Figure 5 presents the stability results (under continuous illumination at MPPT and ambient conditions (temperature ~ 30 ℃ and relative humidity (RH) ~ 50 %) for the encapsulated HaPSCs with CuI or PEDOT:PSS as an HTL. It also has a comparable device performance (Fig. S7). Note that both HTLs are processed with aqueous precursor at ambient conditions. We found that the HaPSC with CuI demonstrated improved air stability compared to the device with PEDOT:PSS. This result is analogous to other reports.[27,28] We found that the device with CuI retained ~90% of its initial efficiency after 15 days, while that for the device with PEDOT:PSS decreased to 70% in a faster rate. It is noticed that the J_{SC} for the PEDOT:PSS device dropped rapidly while other parameters decreased gradually. The lower stability of the device with PEDOT:PSS is related to the chemistry of PEDOT:PSS[44,45] as well as the intrinsic instability of the HaP layer.[23,41] It has been documented that the hygroscopic and acidic properties of PEDOT:PSS is detrimental for the device durability whereas the CuI is benefited from its excellent ambient stability and hydrophobic nature.[46] Thus, this work suggests that the CuI film processed with an ammoniated aqueous solution can be an alternative to the PEDOT:PSS to get efficient and stable inverted HaPSC.

4. Conclusions

We fabricated the perovskite device with ammoniated aqueous solution-processed CuI film and studied the material growth optoelectronic properties. The morphology and crystallinity of perovskite films grown on the CuI layer are affected by the morphology of the CuI film.

A device efficiency of ~14.21% was achieved for the CuI based device with high reproducibility. The capacitance analysis revealed the two trap centers of 0.527 eV and 0.332 eV in the CuI-based device suggesting dominant recombination in the perovskite bulk. It is worth noting that the HaPSC with CuI exhibits superior device stability compared to aqueous PEDOT:PSS based devices. This work presents that the low-cost and ammoniated aqueous solution-processed CuI is a promising HTL for efficient and stable inverted HaPSCs and large-scale industrial production.

Supporting Information

The Supporting Information is available on the website.

Images of precursor solution, ultraviolet photoelectron yield spectra, absorption and PL spectra, steady state device parameters, current-voltage characteristics; J-V-I, J-V-T, capacitance spectra (C-f-T), and J-V characteristics of HaPSCs with CuI or PEDOT:PSS.

Conflicts of interest

There are no conflicts to declare.

Acknowledgements

This work was supported, in part, by the MEXT Program for Development of Environmental Technology using Nanotechnology and the Japanese Society for the Promotion of Science (JSPS), KAKENHI (JP16K06285). Dr. D. B. Khadka also acknowledges The Hitachi Global Foundation, Kurata Grant (#1391) for research funding.

References

[1] T.M. Brenner, D.A. Egger, L. Kronik, G. Hodes, D. Cahen, Hybrid organic-inorganic perovskites: low-cost semiconductors with intriguing charge-transport properties, Nat. Rev. Mater. 1 (2016) 15007. doi:10.1038/natrevmats.2015.7.

[2] A. Kojima, K. Teshima, Y. Shirai, T. Miyasaka, Organometal Halide Perovskites as Visible-Light Sensitizers for Photovoltaic Cells, J. Am. Chem. Soc. 131 (2009) 6050.

[3] M. Saliba, Polyelemental, Multicomponent Perovskite Semiconductor Libraries through Combinatorial Screening, Adv. Energy Mater. 9 (2019) 1803754. doi:10.1002/aenm.201803754.

[4] W.-J. Yin, J.-H. Yang, J. Kang, Y. Yan, S.-H. Wei, Halide perovskite materials for solar cells: a theoretical review, J. Mater. Chem. A. 3 (2015) 8926–8942. doi:10.1039/C4TA05033A.

[5] L. Calió, S. Kazim, M. Grätzel, S. Ahmad, Hole-Transport Materials for Perovskite Solar Cells, Angew. Chemie - Int. Ed. 55 (2016) 14522–14545. doi:10.1002/anie.201601757.

[6] K.T. Cho, S. Paek, G. Grancini, C. Roldan-Carmona, P. Gao, Y. Lee, M.K. Nazeeruddin, Highly efficient perovskite solar cells with a compositionally engineered perovskite/hole transporting material interface, Energy Environ. Sci. 10 (2017) 621–627. doi:10.1039/C6EE03182J.

[7] M.B. Islam, M. Yanagida, Y. Shirai, Y. Nabetani, K. Miyano, Highly stable semi-transparent MAPbI3 perovskite solar cells with operational output for 4000 h, Sol.

Energy Mater. Sol. Cells. 195 (2019) 323–329. doi:10.1016/j.solmat.2019.03.004.

[8] C. Bi, Q. Wang, Y. Shao, Y. Yuan, Z. Xiao, J. Huang, Non-wetting surface-driven high-aspect-ratio crystalline grain growth for efficient hybrid perovskite solar cells., Nat. Commun. 6 (2015) 7747. doi:10.1038/ncomms8747.

[9] D.B. Khadka, Y. Shirai, M. Yanagida, K. Miyano, Unraveling the Impacts Induced by Organic and Inorganic Hole Transport Layers in Inverted Halide Perovskite Solar Cells, ACS Appl. Mater. Interfaces. 11 (2019) 7055–7065. doi:10.1021/acsami.8b20924.

[10] J. You, L. Meng, T.-B. Song, T.-F. Guo, Y. Yang, W.-H. Chang, Z. Hong, H. Chen, H. Zhou, Q. Chen, Y. Liu, N. De Marco, Y. Yang, Improved air stability of perovskite solar cells via solution-processed metal oxide transport layers, Nat. Nanotechnol. 11 (2016) 75–81. doi:10.1038/nnano.2015.230.

[11] Q. Jiang, L. Zhang, H. Wang, X. Yang, J. Meng, H. Liu, Z. Yin, J. Wu, X. Zhang, J. You, Enhanced electron extraction using SnO2 for high-efficiency planar-structure HC(NH2)2PbI3-based perovskite solar cells, Nat. Energy. 2 (2017) 16177. doi:10.1038/nenergy.2016.177.

[12] X. Wan, Y. Jiang, Z. Qiu, H. Zhang, X. Zhu, I. Sikandar, X. Liu, X. Chen, B. Cao, Zinc as a New Dopant for NiO x -Based Planar Perovskite Solar Cells with Stable Efficiency near 20%, ACS Appl. Energy Mater. 1 (2018) 3947–3954. doi:10.1021/acsaem.8b00671.

[13] W. Chen, Y. Wu, Y. Yue, J. Liu, W. Zhang, X. Yang, H. Chen, E. Bi, I. Ashraful, M. Grätzel, L. Han, Efficient and stable large-area perovskite solar cells with inorganic

charge extraction layers, Science (80-.). 350 (2015) 944–948. doi:10.1126/science.aad1015.

[14] A. Huang, L. Lei, Y. Chen, Y. Yu, Y. Zhou, Y. Liu, S. Yang, S. Bao, R. Li, P. Jin, Minimizing the energy loss of perovskite solar cells with Cu+ doped NiOx processed at room temperature, Sol. Energy Mater. Sol. Cells. 182 (2018) 128–135. doi:10.1016/j.solmat.2018.01.025.

[15] H. Rao, S. Ye, W. Sun, W. Yan, Y. Li, H. Peng, Z. Liu, Z. Bian, Y. Li, C. Huang, A 19.0% efficiency achieved in CuO x -based inverted CH 3 NH 3 PbI 3−x Cl x solar cells by an effective Cl doping method, Nano Energy. 27 (2016) 51–57. doi:10.1016/j.nanoen.2016.06.044.

[16] S. Chatterjee, A.J. Pal, Introducing Cu2O thin films as a hole-transport layer in efficient planar perovskite solar cell structures, J. Phys. Chem. C. 120 (2016) 1428–1437. doi:10.1021/acs.jpcc.5b11540.

[17] X. Yao, J. Qi, W. Xu, X. Jiang, X. Gong, Y. Cao, Cesium-Doped Vanadium Oxide as the Hole Extraction Layer for Efficient Perovskite Solar Cells, ACS Omega. 3 (2018) 1117–1125. doi:10.1021/acsomega.7b01944.

[18] K. Zhao, G.O. Ngongang Ndjawa, L.K. Jagadamma, A. El Labban, H. Hu, Q. Wang, R. Li, M. Abdelsamie, P.M. Beaujuge, A. Amassian, Highly efficient organic solar cells based on a robust room-temperature solution-processed copper iodide hole transporter, Nano Energy. 16 (2015) 458–469. doi:10.1016/j.nanoen.2015.07.018.

[19] W. Sun, H. Peng, Y. Li, W. Yan, Z. Liu, Z. Bian, C. Huang, Solution-processed copper iodide as an inexpensive and effective anode buffer layer for polymer solar

cells, J. Phys. Chem. C. 118 (2014) 16806–16812. doi:10.1021/jp412784q.

[20] G.R.A. Kumara, S. Kaneko, M. Okuya, K. Tennakone, Fabrication of dye-sensitized solar cells using triethylamine hydrothiocyanate as a CuI crystal growth inhibitor, Langmuir. 18 (2002) 10493–10495. doi:10.1021/la020421p.

[21] C. Yang, M. Kneiß, M. Lorenz, M. Grundmann, Room-temperature synthesized copper iodide thin film as degenerate p-type transparent conductor with a boosted figure of merit, Proc. Natl. Acad. Sci. 113 (2016) 12929–12933. doi:10.1073/pnas.1613643113.

[22] J.A. Christians, R.C.M. Fung, P. V Kamat, An inorganic hole conductor for Organo-lead halide perovskite solar cells. improved hole conductivity with copper iodide, J. Am. Chem. Soc. 136 (2014) 758–764. doi:10.1021/ja411014k.

[23] H. Wang, Z. Yu, J. Lai, X. Song, X. Yang, A. Hagfeldt, L. Sun, One plus one greater than two: high-performance inverted planar perovskite solar cells based on a composite CuI/CuSCN hole-transporting layer, J. Mater. Chem. A. 6 (2018) 21435–21444. doi:10.1039/C8TA07332E.

[24] J. Liu, S.K. Pathak, N. Sakai, R. Sheng, S. Bai, Z. Wang, H.J. Snaith, Identification and Mitigation of a Critical Interfacial Instability in Perovskite Solar Cells Employing Copper Thiocyanate Hole-Transporter, Adv. Mater. Interfaces. 3 (2016) 1600571. doi:10.1002/admi.201600571.

[25] S. Ye, W. Sun, Y. Li, W. Yan, H. Peng, Z. Bian, Z. Liu, C. Huang, CuSCN-Based Inverted Planar Perovskite Solar Cell with an Average PCE of 15.6%, Nano Lett. 15 (2015) 3723–3728. doi:10.1021/acs.nanolett.5b00116.

[26] M. Jung, S.-G. Ji, G. Kim, S. Il Seok, Perovskite precursor solution chemistry: from fundamentals to photovoltaic applications, Chem. Soc. Rev. 48 (2019) 2011–2038. doi:10.1039/C8CS00656C.

[27] W. Chen, L. Deng, S. Dai, X. Wang, C. Tian, X. Zhan, S. Xie, R. Huang, L. Zheng, Low-cost solution-processed copper iodide as an alternative to PEDOT: PSS hole transport layer for efficient and stable inverted planar heterojunction perovskite solar cells, J. Mater. Chem. A. 3 (2015) 19353–19359. doi:10.1039/C5TA05286F.

[28] W. Sun, S. Ye, H. Rao, Y. Li, Z. Liu, L. Xiao, Z. Chen, Z. Bian, C. Huang, Room-temperature and solution-processed copper iodide as the hole transport layer for inverted planar perovskite solar cells, Nanoscale. 8 (2016) 15954–15960. doi:10.1039/c6nr04288k.

[29] J. Minsu, K.Y. Chan, J.N. Joong, Y.W. Seok, S. Jangwon, N.J. Hong, I.S. Sang, Thermal Stability of CuSCN Hole Conductor-Based Perovskite Solar Cells, ChemSusChem. 9 (2016) 2592–2596. doi:10.1002/cssc.201600957.

[30] D.B. Khadka, Y. Shirai, M. Yanagida, K. Miyano, Unraveling the impacts induced by organic and inorganic hole transport layers in inverted halide perovskite solar cells, ACS Appl. Mater. Interfaces. 11 (2019) 7055–7065. doi:10.1021/acsami.8b20924.

[31] D.B. Khadka, Y. Shirai, M. Yanagida, T. Masuda, K. Miyano, Enhancement in efficiency and optoelectronic quality of perovskite thin films annealed in MACl vapor, Sustain. Energy Fuels. 1 (2017) 755–766. doi:10.1039/C7SE00033B.

[32] B.L. Zhu, X.Z. Zhao, Transparent conductive CuI thin films prepared by pulsed laser

deposition, Phys. Status Solidi Appl. Mater. Sci. 208 (2011) 91–96. doi:10.1002/pssa.201026239.

[33] M.I. Saidaminov, A.L. Abdelhady, B. Murali, E. Alarousu, V.M. Burlakov, W. Peng, I. Dursun, L. Wang, Y. He, G. Maculan, A. Goriely, T. Wu, O.F. Mohammed, O.M. Bakr, High-quality bulk hybrid perovskite single crystals within minutes by inverse temperature crystallization, Nat. Commun. 6 (2015) 7586. doi:10.1038/ncomms8586.

[34] Q. He, K. Yao, X. Wang, X. Xia, S. Leng, F. Li, Room-Temperature and Solution-Processable Cu-Doped Nickel Oxide Nanoparticles for Efficient Hole-Transport Layers of Flexible Large-Area Perovskite Solar Cells, ACS Appl. Mater. Interfaces. 9 (2017) 41887–41897. doi:10.1021/acsami.7b13621.

[35] D.B. Khadka, Y. Shirai, M. Yanagida, K. Miyano, Tailoring the film morphology and interface band offset of caesium bismuth iodide-based Pb-free perovskite solar cells, J. Mater. Chem. C. 7 (2019) 8335–8343. doi:10.1039/C9TC02181G.

[36] M. Stolterfoht, P. Caprioglio, C.M. Wolff, J.A. Márquez, J. Nordmann, S. Zhang, D. Rothhardt, U. Hörmann, Y. Amir, A. Redinger, L. Kegelmann, F. Zu, S. Albrecht, N. Koch, T. Kirchartz, M. Saliba, T. Unold, D. Neher, The impact of energy alignment and interfacial recombination on the internal and external open-circuit voltage of perovskite solar cells, Energy Environ. Sci. 12 (2019) 2778–2788. doi:10.1039/c9ee02020a.

[37] S.R. Cowan, A. Roy, A.J. Heeger, Recombination in polymer-fullerene bulk heterojunction solar cells, Phys. Rev. B. 82 (2010) 245207.

doi:10.1103/PhysRevB.82.245207.

[38] D.B. Khadka, Y. Shirai, M. Yanagida, J.W. Ryan, K. Miyano, Exploring the effects of interfacial carrier transport layers on device performance and optoelectronic properties of planar perovskite solar cells, J. Mater. Chem. C. 5 (2017) 8819–8827. doi:10.1039/C7TC02822A.

[39] D. Bryant, S. Wheeler, B.C. O'Regan, T. Watson, P.R.F. Barnes, D. Worsley, J. Durrant, Observable Hysteresis at Low Temperature in "hysteresis Free" Organic-Inorganic Lead Halide Perovskite Solar Cells, J. Phys. Chem. Lett. 6 (2015) 3190–3194. doi:10.1021/acs.jpclett.5b01381.

[40] W.L. Leong, Z. Ooi, D. Sabba, C. Yi, S.M. Zakeeruddin, M. Graetzel, J.M. Gordon, E.A. Katz, N. Mathews, Identifying Fundamental Limitations in Halide Perovskite Solar Cells, Adv. Mater. 28 (2016) 2439–2445. doi:10.1002/adma.201505480.

[41] D.B. Khadka, Y. Shirai, M. Yanagida, K. Miyano, Degradation of Encapsulated Perovskite Solar Cells Driven by Deep Trap States and Interfacial Deterioration, J. Mater. Chem. C. 6 (2018) 162–170. doi:10.1039/C7TC03733C.

[42] T. Walter, R. Herberholz, C. Müller, H.W. Schock, Determination of defect distributions from admittance measurements and application to Cu(In,Ga)Se2 based heterojunctions, J. Appl. Phys. 80 (1996) 4411–4420. doi:10.1063/1.363401.

[43] D.B. Khadka, S.Y. Kim, J.H. Kim, A Nonvacuum Approach for Fabrication of Cu2ZnSnSe4/In2S3 Thin Film Solar Cell and Optoelectronic Characterization Characterization, J. Phys. Chem. C. 119 (2015) 12226–12235. doi:10.1021/acs.jpcc.5b03193.

[44] H. Choi, C.-K. Mai, H.-B. Kim, J. Jeong, S. Song, G.C. Bazan, J.Y. Kim, A.J. Heeger, Conjugated polyelectrolyte hole transport layer for inverted-type perovskite solar cells, Nat. Commun. 6 (2015) 7348. doi:10.1038/ncomms8348.

[45] R.A. Belisle, P. Jain, R. Prasanna, T. Leijtens, M.D. McGehee, Minimal Effect of the Hole-Transport Material Ionization Potential on the Open-Circuit Voltage of Perovskite Solar Cells, ACS Energy Lett. 1 (2016) 556–560. doi:10.1021/acsenergylett.6b00270.

[46] S. Shao, J. Liu, J. Zhang, B. Zhang, Z. Xie, Y. Geng, L. Wang, Interface-Induced Crystalline Ordering and Favorable Morphology for Efficient Annealing-Free Poly(3-hexylthiophene): Fullerene Derivative Solar Cells, ACS Appl. Mater. Interfaces. 4 (2012) 5704–5710. doi:10.1021/am3017653.